The Karman vortex trail and flow behind a circular cylinder

Lawrence Sirovich
Department of Applied Mathematics, Brown University, Providence, Rhode Island 02912

(Received 11 February 1985; accepted 22 May 1985)

Recent measurements by Sreenivasen [*Frontiers in Fluid Mechanics* (Springer, New York, 1985), pp. 41–67] have shown the presence of temporal frequencies (other than the shedding frequency) in the vortex wake generated by a circular cylinder. It is shown here that these modes of oscillation can be described in terms of the classical analysis of the von Karman vortex trail. A comparison of theory with experiment identifies the individually excited modes.

I. INTRODUCTION

Recently Sreenivasen[1] has shown through careful measurements of flow past a circular cylinder in the regime of vortex shedding ($35 < \mathrm{Re} < 10^4$) that a number of interesting effects are at work. Particularly, he shows that while this regime is not usually regarded as turbulent, the Ruelle–Takens[2] "route to chaos" does occur if relatively low values of the velocity power spectrum are scrutinized. The first step of this route is limit cycle behavior which in the present case is vortex shedding, and is generally accepted as first occurring for $30 < \mathrm{Re} < 40$.[3–5] The next step is a two-torus motion in which two distinct frequencies are present. Such is the case, as shown in Fig. 1 (furnished to the author by Sreenivasen), at a Reynolds number of 58. Here f_1 represents the vortex shedding frequency, while f_2 is a clearly discernible second frequency. (The "combination tones" $f_1 \pm f_2$, $2f_1$, $2f_1 \pm f_2$,... are of course produced by nonlinearities.)

The purpose of this article is to show that such effects may be given a satisfactory explanation that lies within the classical analysis of the Karman vortex trail.[6]

II. STABILITY OF THE KARMAN VORTEX TRAIL

Consider the Karman vortex trail as depicted in Fig. 2. As is well-known the configuration is linearly unstable unless the vortices are staggered as in the figure, and the "aspect ratio" satisfies

$$k = h/l = (1/\pi)\sinh^{-1} 1 \approx 0.281. \tag{1}$$

In this case the trail is neutrally stable to all perturbations. A nominal frequency of oscillation in this case is given by

$$\Omega_0 = (\kappa/8l^2)\ \mathrm{Hz}, \tag{2}$$

where κ is the vortex strength, as indicated in Fig. 2. To arrive at this value of frequency, a group of four neighboring vortices are perturbed and this pattern is periodically repeated (see Fig. 2). Equation (2) then follows from essentially a normal mode analysis. As is discussed later, other natural frequencies are possible. Equation (8) is the most often mentioned value and we use it for illustration and normalization.

It was erroneously concluded by von Karman that if (1) holds the vortex trail is stable. Kochin[7,8] has shown, through the construction of a Lyapunov function, that the exact (nonlinear) dynamical equations for the four-group perturbation give rise to unstable solutions. Mention should be made of the treatment of Domm,[9] who in a related context carries the analysis through quadratic terms and demonstrates (an amplitude-dependent) exponential growth.

A numerical integration of the four-group equations proves to be revealing. Figure 3 shows the relative motion of two typical vortices, according to the exact nonlinear equations, after a relatively large perturbation of 20%. The trace begins to diverge after roughly ten oscillations, but as we see later this corresponds to the shedding of roughly 250 vortex pairs—well above the number found in experiment.

III. FLOW BEHIND A CIRCULAR CYLINDER

Next we review, in brief, the relationship of the vortex trail to flow behind a cylinder. To be specific, we imagine uniform flow U_0 in the positive x direction past a circular cylinder. The shed vortices have the sense shown in Fig. 2. For this case the vortex trail moves to the left, relative to a fluid at rest at infinity, with speed[6]

$$U_s = \kappa/(2\sqrt{2}l). \tag{3}$$

Thus the velocity of the vortex trail relative to the upstream is

$$U_0 - U_s = U_0 - \kappa/(2l\sqrt{2}) \tag{4}$$

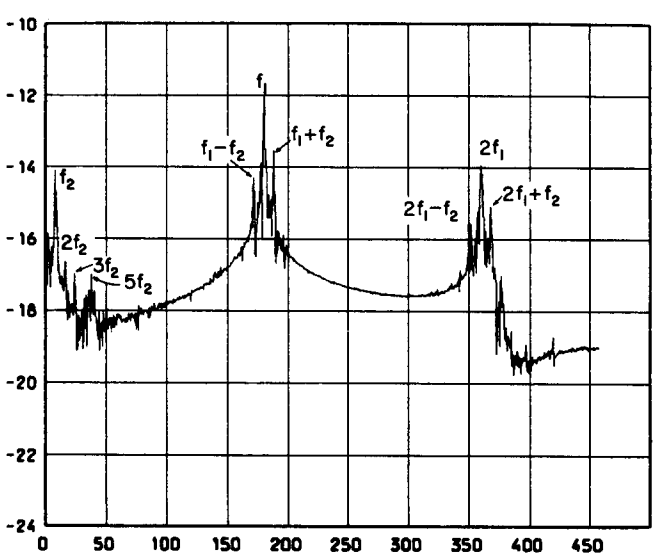

FIG. 1. Normalized frequency spectrum for the streamwise velocity at Re = 58. Shedding frequency, $f_1 \approx 181$ Hz. Second frequency, $f_2 \approx 7.8$. Rotation number $f_2/f_1 \approx 0.043$. (This figures replaces Fig. 3 of Ref. 1, which was incorrectly included in that paper.)

 0031-9171/85/092723-04$01.90 © 1985 American Institute of Physics

Downloaded 09 Jun 2008 to 146.203.28.10. Redistribution subject to AIP license or copyright; see http://pof.aip.org/pof/copyright.jsp

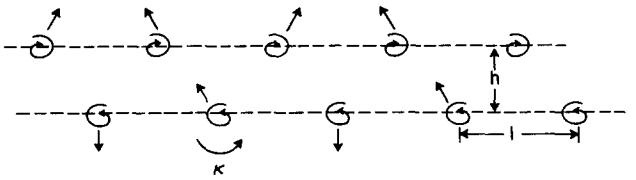

FIG. 2. Schematic of a vortex trail aspect ratio h/l and circulation κ. Arrows indicate a four-group perturbation (see text).

and the frequency of shedding is

$$\Omega = (U_0 - U_s)/l = (U_0/l)(1 - U_s/U_0). \tag{5}$$

Thus from (2) the frequency ratio, or rotation number, is

$$\frac{\Omega_0}{\Omega} = \frac{U_s/U_0}{2^{3/2}(1 - U_s/U_0)}. \tag{6}$$

Equation (6) cannot be applied without a knowledge of U_s, and this quantity which varies with downstream position is difficult to measure. In order to eliminate U_s we follow von Karman,[5] who through the use of a momentum balance argument relates the drag experienced by the cylinder to the vortex trail,

$$C_D = \frac{\kappa^2}{l\pi d U_0^2} + \frac{2\kappa h}{d l U_0^2}(U_0 - 2U_s)$$

$$\approx \frac{l}{d}\left[1.588\frac{U_s}{U_0} - 0.628\left(\frac{U_s}{U_0}\right)^2\right]. \tag{7}$$

Here C_D is the usual dimensionless drag coefficient and d is the cylinder diameter. Although it has been stated that (7) "checks fairly well with measurement,"[10] the evidence cannot be regarded as overwhelming.

IV. ROTATION NUMBER

In order to compare the rotation number with the measured value, we introduce the Strouhal number

$$S = \Omega d/U_0. \tag{8}$$

Then (5) and (7) can be combined to give

$$SC_D = (1 - U_s/U_0) \times [1.588(U_s/U_0) - 0.628(U_s/U_0)^2]. \tag{9}$$

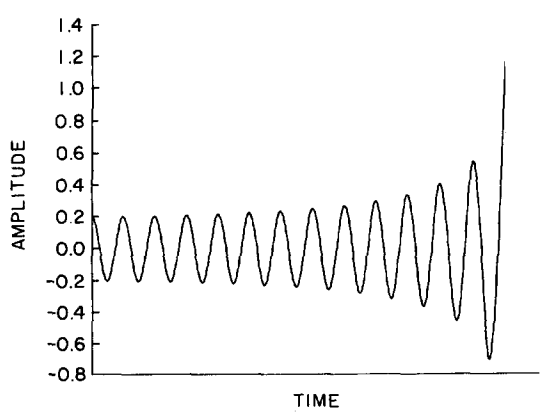

FIG. 3. Exact numerical integration of the nonlinear equations (see Kochin[7]) for the four-group perturbation. The ordinate measures the normalized relative perturbation of two vortices.

We adopt the view that the left-hand side of (9) is a function of the Reynolds number Re which is determined by experiment. Once this is done, the cubic is solved for U_s/U_0 and the result substituted into (6).

For the case depicted in Fig. 1, $d = 0.079$ cm, $U_0 = 110$ cm/sec, $\Omega = 181$ Hz so that

$$S = 0.130. \tag{10}$$

At the same Reynolds number, Re = 58, the drag coefficient is[4]

$$C_D = 1.43 \tag{11}$$

and substitution into (9) yields

$$U_s/U_0 = 0.153. \tag{12}$$

If this value is substituted into (6) we obtain the rotation number

$$\Omega_0/\Omega = 0.064. \tag{13}$$

This is to be compared with the value of 0.043, which is measured by Sreenivasen.[1] In view of the seemingly loose connection between theory and experiment, the 50% discrepancy of (13) over the measured value might be regarded as tolerable. However, in the following section we show that much closer agreement can be obtained. For the moment we extend the above treatment somewhat.

The above discussion relies on the idea that the drag coefficient C_D is a function of the Reynolds number. This quantity can be obtained from experiment, and in what follows we use the measured values given by Tritton[4] in graphical and tabular form. In the same way the Strouhal number is also furnished by measurement. In fact, for the range of Reynolds numbers considered here, Roshko[11] gives the relationship

$$S = \Omega d/U_0 \approx 0.212 - 4.5/\mathrm{Re}, \quad 50 < \mathrm{Re} < 150, \tag{14}$$

which he states gives a fit to the measurements. [For the case depicted in Fig. 1, Eq. (14) gives 0.134 in contrast with 0.130 in Eq. (10).] If (14) and $C_D(R)$, taken from Tritton,[4] are substituted into (9), it implicitly determines U_s/U_0 as a function of Re. This solution is then introduced into (6), and the result for the rotation number as a function of Reynolds number is plotted in Fig. 4. The heavy black dots refer to data obtained by Sreenivasen.[1] The dashed curves will be explained in the next section.

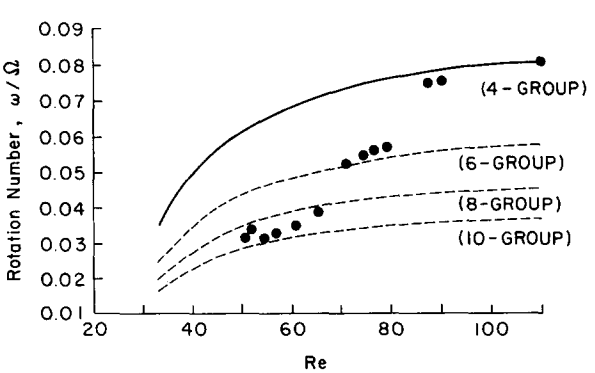

FIG. 4. Plots of rotation number ϕ/Ω versus Reynolds number Re. Continuous curve represents theoretical prediction based on four-group perturbation. Dashed curves are theoretical predictions based on indicated perturbations. Heavy dots represent measurements obtained by Sreenivasen.[1]

Downloaded 09 Jun 2008 to 146.203.28.10. Redistribution subject to AIP license or copyright; see http://pof.aip.org/pof/copyright.jsp

V. MODAL OSCILLATIONS

As has been emphasized, the discussion thus far is based on the special case of the four-group perturbation of the Karman trail. Within the framework of linear theory, one can also explicitly treat periodic perturbations of arbitrary length as well as the aperiodic case. The essential steps are to be found in Lamb.[6] We briefly outline this treatment in a somewhat different way.

The equilibrium positions of vortices in the Karman vortex trail, in the neutrally stable case, are given by

$$Z_m^+ = ml + U_s t + ih/2,$$
$$Z_m^- = (m + \tfrac{1}{2})l + U_s t - ih/2, \tag{15}$$

where U_s is given by (3) and the aspect ratio is given by (1). The $\pm$ superscripts refer to upper and lower rows. In the same notation we denote perturbations from (15) by

$$z_m^\pm = x_m^\pm + iy_m^\pm. \tag{16}$$

The linearized perturbation equations are then given by

$$\frac{d}{dt}\bar{z}_m^\pm = \mp\frac{i\kappa}{2\pi}\sum_k{}' \frac{z_m^\pm - z_k^\pm}{(m-k)^2 l^2} \pm \frac{i\kappa}{2\pi}\sum \frac{z_m^\pm - z_k^+}{[(m-k\mp\tfrac{1}{2})l \pm ih]^2}, \tag{17}$$

where the bar denotes complex conjugation.

To solve (17) introduce the generating functions:

$$\begin{bmatrix} X^+ \\ Y^+ \end{bmatrix} = \sum_m \begin{bmatrix} x_m^+ \\ y_m^+ \end{bmatrix} \exp(im\phi);$$
$$\begin{bmatrix} X^- \\ Y^- \end{bmatrix} = \sum_m \begin{bmatrix} x_m^- \\ y_m^- \end{bmatrix} \exp\left[i\left(m+\frac{1}{2}\right)\phi\right]. \tag{18}$$

For a periodic disturbance the summations are finite. If (18) is introduced into (17), it then follows that

$$\frac{d}{d\tau}\begin{bmatrix}\alpha\\ \beta\end{bmatrix} = \begin{bmatrix} ib & a-c \\ a+c & ib \end{bmatrix}\begin{bmatrix}\alpha\\ \beta\end{bmatrix}, \tag{19}$$

where

$$\alpha = (X^+ + X^-)/2, \quad \beta = (Y^+ - Y^-)/2, \quad \tau = \kappa t/(2\pi l^2), \tag{20}$$

and

$$a = [\phi(2\pi - \phi) - \pi^2]/2,$$
$$c = [\pi^2 \cosh(k\kappa) - \pi\phi\sqrt{2}\cosh k(\pi - \phi)]/2, \tag{21}$$
$$b = [\sqrt{2}\pi\phi \sinh k(\pi - \phi) + \pi^2 \sinh k\phi]/2.$$

The remaining quantities

$$\mu = (X^+ - X^-)/2, \quad \nu = (Y^+ + Y^-)/2 \tag{22}$$

are such that $(\bar{\nu}, \bar{\mu})$ also satisfy (19).

Postulating that $(\alpha, \beta) \propto \exp(i\omega\tau)$, we find

$$\omega = b \pm (c^2 - a^2)^{1/2} = \omega^\pm(\phi). \tag{23}$$

When $\phi = \pi$,

$$\omega^+ = \omega^- = \pi^2/2 = \omega_0. \tag{24}$$

For the moment we depart from the convention of expressing all frequencies in Hz. For example (24), if expressed in Hz, gives $\pi/4$, which is equal to (2) under the temporal normalization given in (20). This should not lead to confusion since we will be interested in the frequency ratio $\omega^\pm/\omega_0$, given in Fig. 5. [The other two roots, which follow from (22), yield the negatives of $\omega^\pm$.]

The plot of rotation number given in Fig. 4 represents (6) and is based on the value of frequency given by (2) [or (24)]. Rotation number curves, corresponding to other allowed values of the perturbation frequency, Eq. (23), are obtained from (6) by multiplying it with the frequency ratio,

$$\nu^\pm(\phi) = \omega^\pm/\omega_0, \tag{25}$$

as given in Fig. 5. Thus in Fig. 4 we indicate by the dashed curves those obtained from multiplying by: $\nu^-(2\pi/3)$, a six-group mode; $\nu^-(\pi/4)$, an eight mode; and $\nu^-(2\pi/5)$, a ten-group mode. Similar curves obtained from the ω^+ mode do not fit the data as well and a moderately convincing argument may be given that implies that the ω^- mode is mainly generated in the experimental situation.

In view of the agreement of the modal curves of Fig. 4 with experiment, it may be worthwhile examining future measurements to see if the observed oscillations conform to the corresponding modal disturbances.

VI. DISCUSSION

We comment on the presence of additional frequencies and "windows of chaos" which Sreenivasen[1] finds. As the above discussion indicates, a continuum of possible frequencies are present in an arbitrary disturbance. Vortex shedding is the driving mechanism of the phenomenon. It both creates the vortex street and the perturbations. The excitation of additional modes and hence the appearance of additional frequencies is, in general, likely. When resonances are struck chaotic behavior can be expected. Fluctuation energies are small compared to the energy of the street itself and little interaction should occur. In fact, Sreenivasen[1] finds only small changes in the shedding frequency as the principal mode of oscillation makes the sharp jumps shown in Fig. 4. (These jumps are separated by "windows of chaos.")

In attempting to connect the theoretical discussion based on the Karman trail with laboratory measurements of flow behind a cylinder, many distinctions appear. With von Karman we can regard the vortex trail as depicting the asymptotic flow downstream of the body. However, viscous effects are sure to play an increasingly important role in this

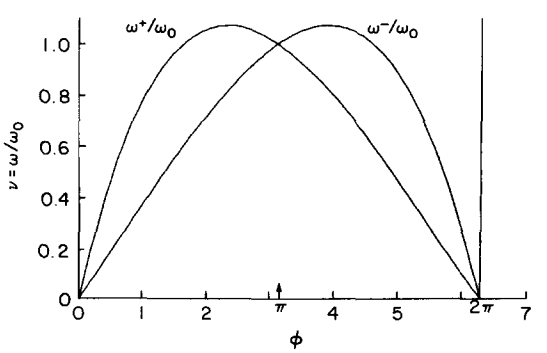

FIG. 5. Dispersion relation showing possible oscillation frequencies for the vortex trail. Frequencies have been normalized with respect to the four-group frequency ω_0. Abscissa ϕ is the angular wavenumber.

Downloaded 09 Jun 2008 to 146.203.28.10. Redistribution subject to AIP license or copyright; see http://pof.aip.org/pof/copyright.jsp

limit. Another serious distinction rests on the fact that the classical stability analysis refers to an initial value problem, viz., the evolution of a perturbation to an unbounded vortex trail. But in experiment the perturbation is introduced by the boundary and the trail is at best half-infinite (the fact that long range "forces" are at work further underlines this distinction). Perhaps connected to this same point about boundary versus initial value problems is the lack of any truly satisfactory explanation as to why the vortex trail should seek out its least unstable configuration. All these criticisms withstanding, the closeness of the results that follow from the Karman trail to measured values make the agreement too coincidental to overlook.

ACKNOWLEDGMENTS

The author wishes to express his appreciation to Phillip Saffman for pointing out Ref. 9 and to Bruce Knight for several enlightening discussions. Special thanks are due to K. R. Sreenivasen for introducing the author to the problem, for enlightening conversations, and for his generosity in supplying the author with figures and data.

[1]K. R. Sreenivasen, in *Frontiers in Fluid Mechanics*, edited by S. H. Davis and J. L. Lumley (Springer, New York, 1985), pp. 41–67.
[2]D. Ruelle and F. Takens, Comm. Math. Phys. **20**, 167 (1971).
[3]S. Taneda, J. Phys. Soc. Jpn. **11**, 302 (1956).
[4]D. J. Tritton, J. Fluid Mech. **6**, 547 (1959).
[5]S. Goldstein, *Modern Developments in Fluid Mechanics* (Dover, New York, 1965), Vol. II, Sec. 247.
[6]H. Lamb, *Hydrodynamics* (Dover, New York, 1945), Sec. 156.
[7]N. E. Kochin, C. R. (Dokl.) Acad. Sci. URSS **24**, 18 (1939).
[8]N. E. Kochin, I. A. Kibel', and N. V. Roze, *Theoretical Hydrodynamics* (Interscience, New York, 1964), Sec. 5.21.
[9]U. Domm, Z. Angew. Math. Mech. **36**, 367 (1956).
[10]T. von Karman and M. Burgers, in *Aerodynamic Theory*, edited by W. F. Durand (Dover, New York, 1963), Vol. II, Sec. VII.7.
[11]A. Roshko, N.A.C.A. Report No. 1191, 1954.

Downloaded 09 Jun 2008 to 146.203.28.10. Redistribution subject to AIP license or copyright; see http://pof.aip.org/pof/copyright.jsp